Global and Planetary Change 193 (2020) 103288

Contents lists available at ScienceDirect

Global and Planetary Change

journal homepage: www.elsevier.com/locate/gloplacha

The 3D thermal field across the Alpine orogen and its forelands and the relation to seismicity

Cameron Spooner[a,b,*], Magdalena Scheck-Wenderoth[a,c], Mauro Cacace[a], Hans-Jürgen Götze[d], Elco Luijendijk[e]

[a] GFZ German Research Centre for Geosciences, Potsdam, Germany
[b] Institute of Earth and Environmental Science, Potsdam University, Potsdam, Germany
[c] Department of Geology, Geochemistry of Petroleum and Coal, RWTH Aachen University, Aachen, Germany
[d] Institute of Geosciences, Christian-Albrechts-University Kiel, Kiel, Germany
[e] Department of Structural Geology and Geodynamics, Georg-August-Universität Göttingen, Göttingen, Germany

ARTICLE INFO

Keywords:
Steady-state
Thermal-field
Europe
Alps
Adria
Seismicity

ABSTRACT

Temperature exerts a first order control on rock strength, principally via thermally activated creep deformation and on the distribution at depth of the brittle-ductile transition zone. The latter can be regarded as the lower bound to the seismogenic zone, thereby controlling the spatial distribution of seismicity within a lithospheric plate. As such, models of the crustal thermal field are important to understand the localisation of seismicity. Here we relate results from 3D simulations of the steady state thermal field of the Alpine orogen and its forelands to the distribution of seismicity in this seismically active area of Central Europe. The model takes into account how the crustal heterogeneity of the region effects thermal properties and is validated with a dataset of wellbore temperatures. We find that the Adriatic crust appears more mafic, through its radiogenic heat values (1.30E-06 W/m3) and maximum temperature of seismicity (600 °C), than the European crust (1.3–2.6E-06 W/m3 and 450 °C). We also show that at depths of < 10 km the thermal field is largely controlled by sedimentary blanketing or topographic effects, whilst the deeper temperature field is primarily controlled by the LAB topology and the distribution and parameterization of radiogenic heat sources within the upper crust.

1. Introduction

One in three people globally live at risk of being affected by seismicity (Pesaresi et al., 2017), therefore the need remains for an increased understanding of the factors that contribute to the localisation of seismicity within the lithosphere. As temperature exerts a first order control on rock strength and seismicity (e.g. Hyndman et al., 1995; Emmerson and McKenzie, 2007), a systematic knowledge of the regional 3D temperature distribution is an essential step towards refining predictions of future seismic hazard.

The study area covered here, the Alps and their forelands, represents one of the most active locations for intraplate seismicity in Europe. Ongoing deformation is primarily driven by the convergence of the European and Adriatic plates in northeast Italy (Restivo et al., 2016), where the Adriatic plate is considered to act as a rigid (i.e. mechanically stiff) indenter, moving northwards with a radial counterclockwise rotation against the weaker European plate (Nocquet and Calais, 2004; Vrabec and Fodor, 2006; Serpelloni et al., 2016).

Recent gravity modelling work of the region (Spooner et al., 2019) have shown that large seismic events cluster across density contrasts within the crust, that represent an inherited crustal configuration of differing petrological and tectono-thermal origin (Schmid et al., 2004). Previously published lithospheric thermal models that cover the entirety of the Alps and their forelands (Tesauro et al., 2009; Limberger et al., 2018) have largely not resolved the vertical and lateral heterogeneities observed mostly in the crustal domains sufficiently well to allow a quantitative assessment of their effects on the resulting temperature distribution. Thermal models that do represent differentiated lithospheric layers and a heterogeneous crust have been published for the Upper Rhine Graben (Freymark et al., 2017) and the Molasse Basin (Przybycin et al., 2014), however these only cover specific subdomains of the area under investigation. In order to further assess how the present-day deformation within the Alpine region is related to the 3D thermal field, we have developed the first 3D steady state lithosphere-scale thermal field of the Alps and their forelands that takes into account the different thermal parameters required to replicate the

* Corresponding author at: GFZ German Research Centre for Geosciences, Potsdam, Germany.
E-mail address: spooner@gfz-potsdam.de (C. Spooner).

https://doi.org/10.1016/j.gloplacha.2020.103288
Received 17 April 2020; Received in revised form 17 July 2020; Accepted 24 July 2020
Available online 31 July 2020

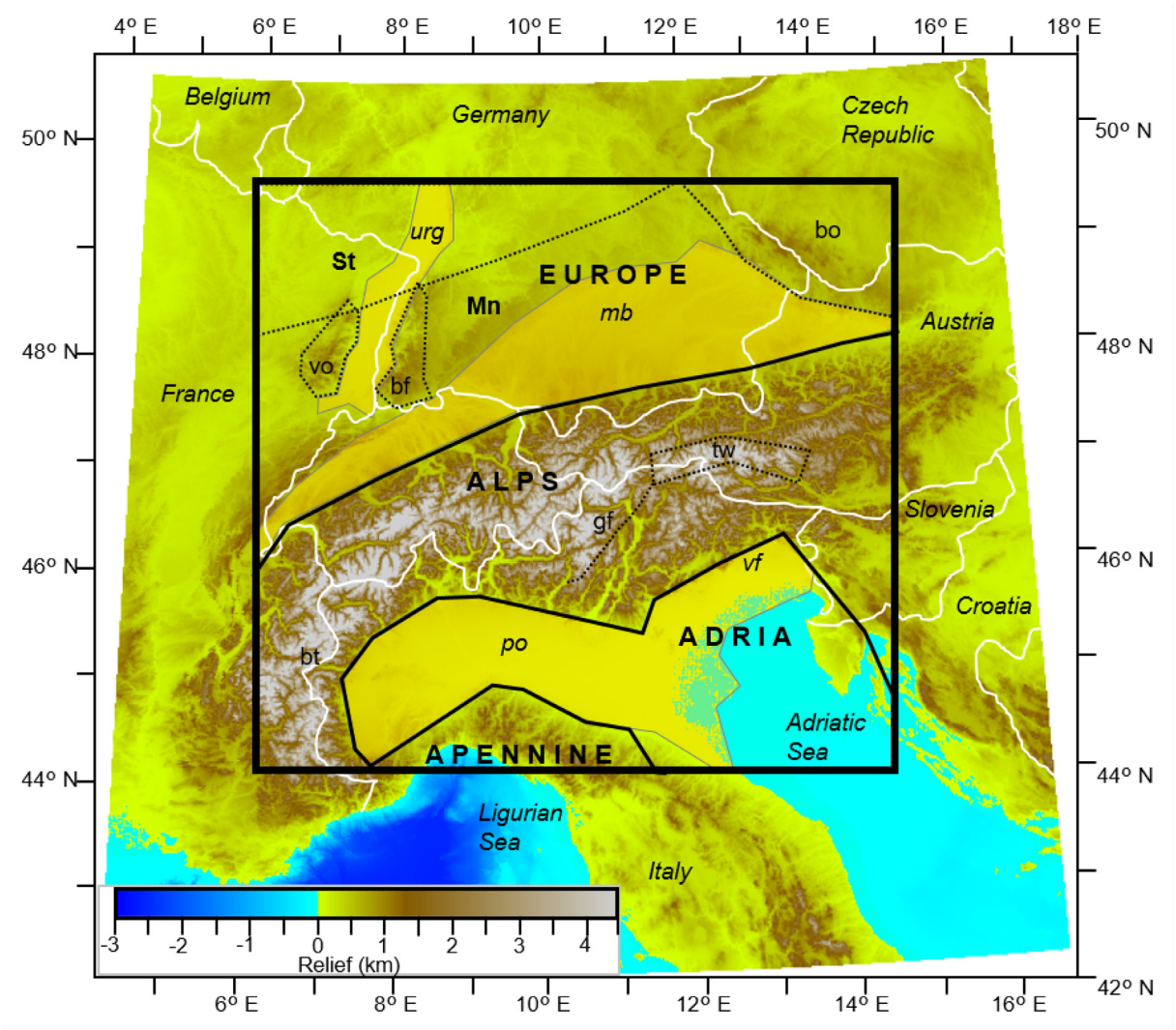

Fig. 1. Topography and bathymetry from Etopo 1 (Amante and Eakins 2009) shown across the Alpine region with the key tectonic features overlain. Study area is indicated with a black box. Solid black lines demark the boundaries of the weakly deformed European and Adriatic plates, the location of the Apennine plate is also marked. Yellow areas bound by a solid grey line indicate the extent of sedimentary basins (urg – Upper Rhine Graben; mb – Molasse Basin; po – Po Basin; vf – Veneto Friuli plane). Dotted black lines indicate the extent of other tectonic features within the model (st – Saxothuringian Variscan domain; mn – Moldanubian Variscan domain; bo – Bohemian Massif; vo – Vosges Massif; bf – Black Forest Massif; tw – Tauern Window; gf – Giudicarie Fault; bt – Brianconnais Terrane). The Adriatic Sea is marked as (AS) in further figures. (For interpretation of the references to colour in this figure legend, the reader is referred to the web version of this article.)

heterogeneous nature of the crust.

1.1. Geological setting

Crustal heterogeneities represent an important feature in the European crust of the north Alpine foreland. Juxtaposition of terrains with differing properties next to one another, such as Moldanubia and Saxothuringia (Babuška and Plomerová, 1992; Freymark et al., 2017), derive from the Carboniferous age Variscan orogeny (Franke, 2000), that assembled crystalline basement presently exposed in the Vosges, Black Forest and Bohemian massifs. Heterogeneity within the Alpine orogen is also very pronounced as a result of the collision of the Adriatic plate with the European plate from the Cretaceous until the present (Handy et al., 2010).

The different parts of the orogen-foreland system (Fig. 1) are presently interpreted according to their provenance and metamorphic history, with the eastern and western Alps being derived from the Adriatic and European plates respectively (Schmid et al., 2004). The Briançonnais crustal block that lies within the western Alps derives from the Iberian plate (Frisch, 1979). The three main depocentres within the region are the Po Basin of the southern foreland, the Molasse Basin of the northern foreland and the Upper Rhine Graben, also within the northern foreland, that formed as part of the European Cenozoic Rift System in the Eocene (Dèzes et al., 2004).

2. Workflow

An existing 3D structure and density model of the Alpine lithosphere made by Spooner et al. (2019), was used to calculate the thermal field of the region. The model covers an area of 660 km × 620 km (shown in Fig. 1) with a horizontal grid resolution of 20 km × 20 km and is the highest resolution 3D structural model of the Alps and foreland region that conforms to seismic and gravity based observations. The vertical resolution is variable, depending on the thickness of the 6 model layers, representing the key structural and density contrasts within the lithosphere: (1) water; (2) unconsolidated sediments (mostly Quaternary); (3) consolidated sediments (mostly Mesozoic); (4) upper crystalline crust; (5) lower crystalline crust; and (6) lithospheric mantle. Each layer (excluding water) is split into distinct domains representing the different tectonic blocks that comprise them. The thickness of each

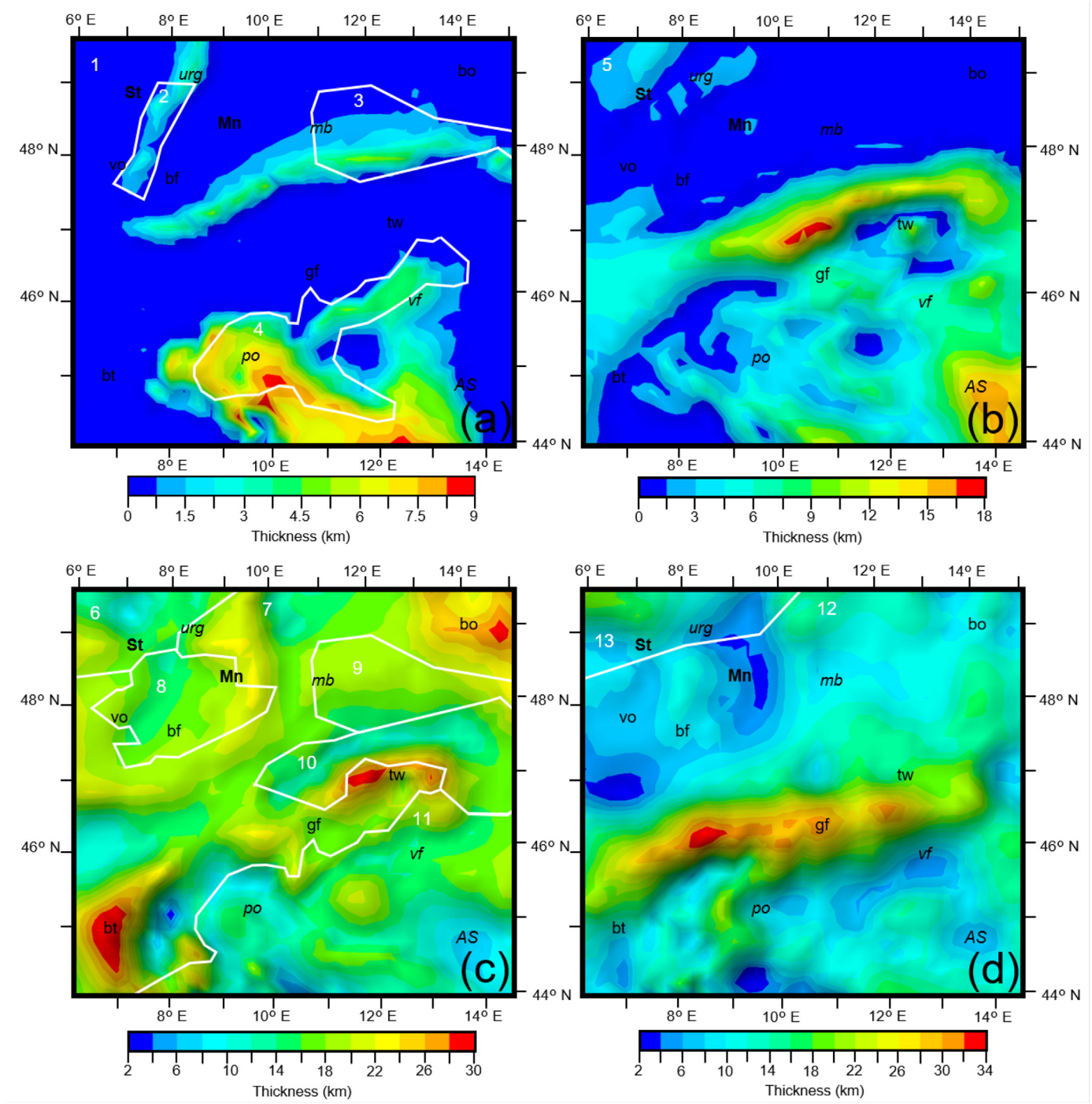

Fig. 2. Thickness of a) unconsolidated sediments (mostly Quaternary), b) consolidated sediments (mostly Mesozoic), c) the upper crystalline crust and d) the lower crystalline crust across the modelled area. Domains of different thermal parameters within each the layer are overlain in white, domain numbers correspond to Table 1. Locations of key tectonic features are overlain (abbreviations shown in Fig. 1 caption).

layer and location of the different domains within them are also shown in Figs. 2 and 3a. No subduction interfaces are included in the model.

Some refinements were made to the original structural model to make it of use for the thermal modelling effort. The water layer was discarded, with the surface representing topography and bathymetry used as the upper limit of the model (shown in Fig. 1) and the Lithosphere-Asthenosphere Boundary (LAB) used as the base of the model (shown in Fig. 3b). Additionally, thick unconsolidated sedimentary layers within the model, were vertically differentiated in terms of thermal parameters into two units to account for porosity changes within these layers due to compaction. As the majority of sedimentary porosity decrease takes place in the upper few kilometres (Allen and Allen, 2013) this transition was implemented at 2 km depth in the Po Basin and 1 km in other areas with less thick deposits of unconsolidated sediments. Further refinement of the model vertical resolution was tested but found to have little effect on the generated thermal field. Accordingly, the vertical resolution was not refined to minimise the computational demand.

A 3D finite element model (32,736 nodes) incorporating these refinements was then used to calculate the 3D conductive steady state thermal field of the study area using GOLEM (Cacace and Jacquey, 2017), a numerical simulator of coupled Thermal-Hydraulic-

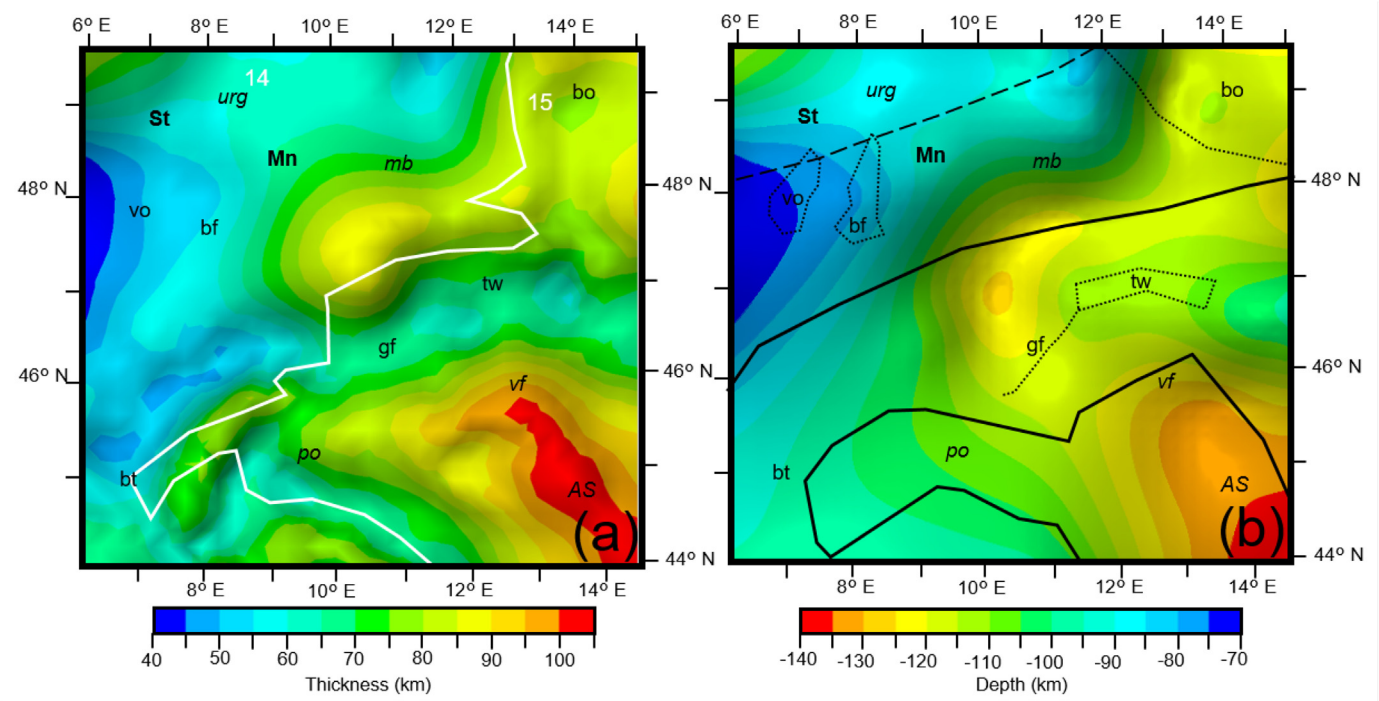

Fig. 3. a) Thickness of the lithospheric mantle layer from the structural model. Domains of different thermal parameters within the layer are overlain in white, domain numbers correspond to Table 1. b) Depth to the LAB from Geissler et al. (2010) across the modelled area. Locations of key tectonic features are overlain (abbreviations shown in Fig. 1 caption).

Mechanical processes. For this study steady state conditions were assumed and the conductive thermal field was calculated. Therefore the conductive heat equation solved for steady state conditions is.

$$0 = \mathrm{div}(\lambda \nabla T) + S \quad (1)$$

where the ∇T is the temperature gradient (K/m), λ is the thermal conductivity (W/mK) and S is the radiogenic heat production (W/m3). The boundary conditions to close the system of equations comprise fixed temperatures along the top and bottom of the model (Dirichlet boundary condition), while all lateral boundaries are considered to be no-flow. The upper thermal boundary condition used (Fig. 4a) corresponds to yearly average surface temperatures, comprising both land and sea floor measurements, from the WOA13 dataset (Locarini et al. Locarnini et al., 2013) the Histalp dataset (Böhm et al., 2009) and the GHCN_CAMS dataset (Fan and Van den Dool, 2008). Temperatures range from −10 °C in the Alps to 16 °C in the Adriatic Sea. The temperature distribution used across the lower thermal boundary condition (see Fig. 4b), is derived from the conversion of shear wave velocities (Priestly and McKenzie, 2006; Meeßen, 2018) from Schaeffer and Lebedev's (2013) SL2013sv dataset, at a depth corresponding to the base of the model. Temperatures range from 1250 °C below the Vosges massif to 1400 °C beneath the Bohemian massif. Although the range of temperatures does not vary significantly, there is an overall spatial correlation between the thermal configuration and the topology of the LAB from the structural model (Spooner et al., 2019), an indication that assuming the LAB derived from seismology (Geissler et al., 2010) as a thermal boundary is justified.

Model validation is carried out by comparing the obtained results against a dataset of measured sub-surface temperatures from across the region. Data for the southern foreland was derived from the Italian National Geothermal Database (Trumpy and Manzella, 2017), for the northern foreland from previously compiled databases of the Upper Rhine Graben (Freymark et al., 2017 and references therein) and the Molasse Basin (Przybycin et al., 2015 and references therein) and within the Alps a dataset compiled by Luijendijk et al. (2020) was used. The combined dataset represents 8120 measurements from the surface down to 7.3 km below sea level, with a mean depth of 1.8 km. Temperature readings of a number of different types were used including, corrected bottom hole, continuous gradient and hot fluid readings, to give as broad a coverage across the region as possible.

In the first modelling stage, each model layer was assigned constant bulk thermal properties, from a range of values using in similar modelling work in the Upper Rhine Graben (Freymark et al., 2017) and Molasse Basin (Przybycin et al., 2015). The ranges of thermal properties tested can be seen in Table. 1. The values used were tested in an iterative fashion, starting at the midpoint of the tested range. The thermal parameters were altered in the lithospheric mantle domains first, at the base of the model, before altering the parameters in each domain successively moving up the layers of the structural model. In layers of the model where radiogenic heat production is expected to be low (unconsolidated sediments, consolidated sediments, lower crust and lithospheric mantle) the thermal conductivity was altered first to fit the measured temperatures before the radiogenic heat value was tweaked to get the best overall fit, with the opposite carried out for the upper crust where the radiogenic heat production is significant.

The best fit thermal field was then compared to the seismic event catalogue of the International Seismological Centre (International Seismological Centre, 2020) for the study area. The catalogue was filtered for events larger than magnitude 2 between January 2000 and January 2018, as the catalogue completeness drops significantly outside of these parameters. This provided a dataset of 4571 seismic events so that relationships between the depth, temperature, and location of seismicity could be explored.

2.1. Methodological limitations

The model generated here represents the first attempt to calculate the 3D steady state thermal field of the Alps and their forelands using different thermal parameters for different tectonic domains, validated with a dataset of wellbore temperatures from across the region, however limitations remain in the current workflow. The resolution of the thermal model generated is a result of the available data sources, which

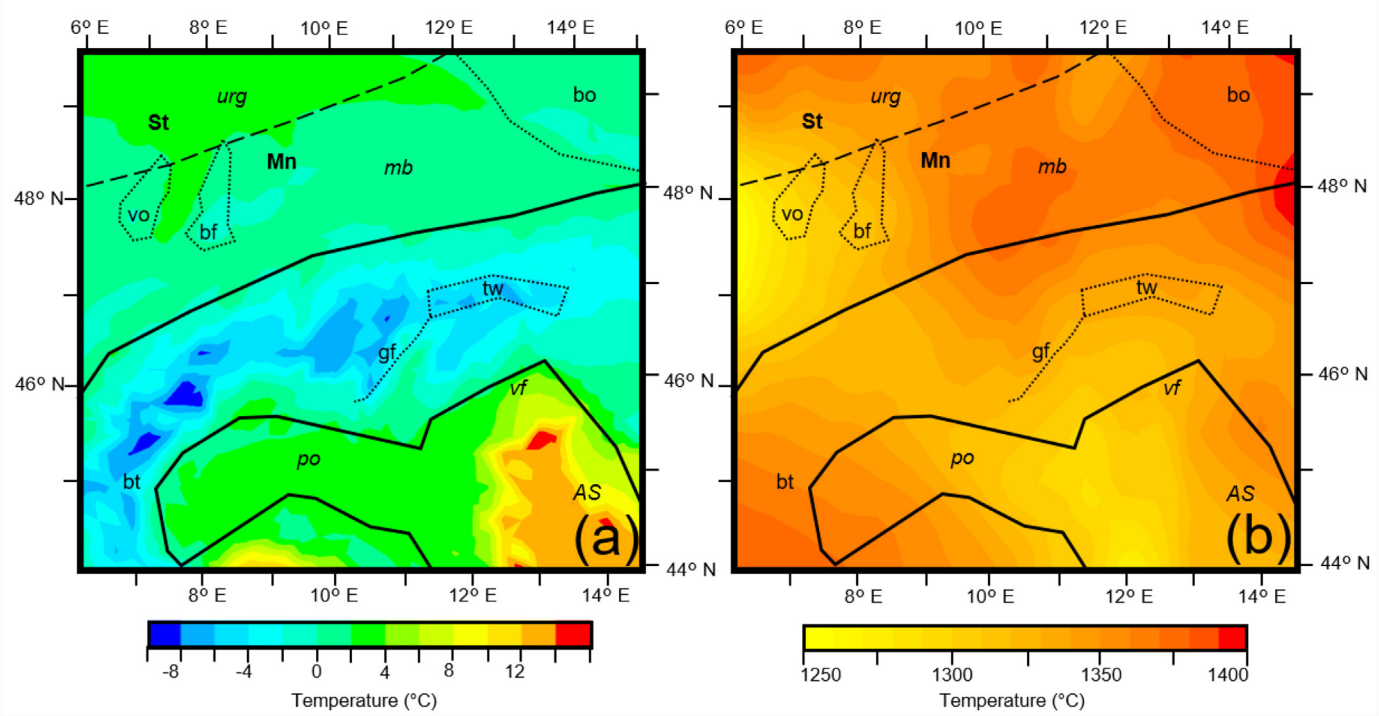

Fig. 4. Temperatures used as the a) upper and b) lower boundary condition for achieving steady state conditions of the thermal model. Temperatures for the upper boundary condition were derived from the WOA13 dataset (Locarini et al. Locarnini et al., 2013) the Histalp dataset (Böhm et al., 2009) and the GHCN_CAMS dataset (Fan and Van den Dool, 2008). Temperatures for the lower boundary conditions were calculated using the LAB of Geissler et al. (2010) and Locarnini et al.'s (2013) SL2013sv dataset. Locations of key tectonic features are overlain (abbreviations shown in Fig. 1 caption).

although state of the art, are limited in their resolution, coverage, and differentiation of Alpine lithospheric units, allowing for a first order comparison of relative thermal trends between large scale crustal features.

The method used to derive thermal parameters produces values representing the bulk average properties of the domain rather than an exact lithology or metamorphic facies. The availability of highly detailed geological information across the entire study area does not support the creation of such a high resolution model, especially at depth. As such, rather than use specific rock values, we test a range of parameter values likely in such a setting. Therefore, indications of lithology derived from the modelled thermal parameters are relative to one another, based upon how thermal parameters act in more mafic or felsic rocks (e.g. Hasterok and Webb, 2017). Despite the sparse nature of higher resolution data, wherever present they have been used to validate the thermal parameters derived from the workflow. Existing P-wave velocity models through the region (e.g. Bleibinhaus and Gebrande, 2006), suggest similar radiogenic heat production values to those we have modelled, when converting using the methodology of Hasterok and Webb (2017).

The thermal field presented here is a first attempt at a truly multi-disciplinary study, integrating data from a wide array of sources.

Table 1
Final thermal parameters used and the tested range for all domains of the structural model.

	Final Bulk Thermal Conductivity	Bulk Thermal Conductivity Range Tested	Final Radiogenic Heat Production	Radiogenic Heat Production Range Tested
	(W/mK)	(W/mK)	(W/m3)	(W/m3)
1. top 1 km Unconsolidated Sediments	2		1.00E-06	
- below 1 km Unconsolidated Sediments	2.3	1.8–3	1.00E-06	1.00E-06
2. top 1 km Unconsolidated Sediments URG	1.1		1.00E-06	
- below 1 km Unconsolidated Sediments URG	1.4	1.1–1.8	1.00E-06	1.00E-06
3. Unconsolidated Sediments Molasse	1.8	1.8–3	1.00E-06	1.00E-06
4. top 2 km Unconsolidated Sediments Po	2		1.00E-06	
- below 2 km Unconsolidated Sediments Po	2.3	1.8–3	1.00E-06	1.00E-06
5. Consolidated Sediments	2.3	2–3.5	1.00E-06	1.00E-06 - 1.30E-06
6. Upper Crust Saxothuringia	3	2.5–4	2.60E-06	1.00E-06 - 2.60E-06
7. Upper Crust Moldanubia and West Alps	2.6	2.3–3.1	1.80E-06	1.00E-06 - 2.60E-06
8. Upper Crust Vosges	2.8	2.3–3.1	2.00E-06	1.00E-06 - 2.60E-06
9. Upper Crust Molasse	2.4	2.3–3.1	1.30E-06	1.00E-06 - 2.60E-06
10. Upper Crust East Alps	2.4	2.2–3.1	1.60E-06	1.00E-06 - 2.60E-06
11. Upper Crust Adria and Apennine	2.4	2.3–3.1	1.30E-06	1.00E-06 - 2.60E-06
12. Lower Crust	2	2–2.7	3.00E-07	1.50E-07 - 7.00E-07
13. Lower Crust Saxothuringia	2.3	2–2.7	6.00E-07	1.50E-07 - 7.00E-07
14. Lithospheric Mantle North West	3	3–3.95	3.00E-08	2.00E-08 - 3.00E-08
15. Lithospheric Mantle South East	3	3–3.95	2.00E-08	2.00E-08 - 3.00E-08

Interpretations used as a basis for the calculated thermal field, including prior work such as the structural model (Spooner et al., 2019) and the thermal parameters assigned to crustal domains, both represent non-unique solutions. To remedy this, at each stage multiple external data sources, such as gravity anomalies, seismicity or wellbore temperatures, have been used for validation.

Limitations of the data used for validation also impacts the modelling effort. The distribution of wellbore measurements represent a significantly heterogeneous data coverage, with regions of interest for geothermal or hydrocarbon exploitation overrepresented and the orogen itself containing sparser coverage. The coverage negates the potential for an accurate deterministic solution to constrain thermal parameters in most regions, and this is further complicated by the required use of different types of measured wellbore temperatures in order to maximise coverage. Therefore, at this time, a qualitatively derived solution for a 3D thermal field of the region represents the best possible solution. In locations where these limitations have been encountered, further mention has been made in the text. Work to quantify the sensitivities of regional thermal parameters to the spread of measurement data is underway.

Another limitation of the workflow is that the model is made with the assumption that the thermal field is in a present day steady state. Steady state assumes that the thermal field has reached equilibrium and changes over time to the thermal field are negated. To progress from steady state to other thermal modelling methods, such as transient thermal fields, where changes through time are calculated, further observations need to be gathered on the contributions of other influencing factors to the thermal field. These include: the effects of hydrothermal convection (e.g. Smith and Chapman, 1983; Ehlers and Chapman, 1999; Sippel et al., 2014); rapid sedimentation rates (Ehlers, 2005); regional glacial history (Mey et al., 2017); present day surface vertical motion (Sternai et al., 2019); and long term exhumation rates (Fox et al., 2016). In locations where these other effects are interpreted to have affected our results, further mention has been made in the text.

3. Results

3.1. Modelled temperature distribution

Fig. 5 illustrates depth slices through the thermal field of the best fit thermal model at 2, 5, 10 and 20 km below sea level. Observations of first order temperature trends at a depth of 2 km, indicate that the pattern of heat distribution correlates spatially to the topography, with the coldest areas in the Ligurian Sea (40 °C) and the hottest areas corresponding to the Alps (140 °C). However, irrespective of similar topographies the western Alps appear generally warmer (140 °C) than the eastern Alps (130 °C). The warmest temperatures outside of the orogen are observed to occur beneath the Upper Rhine Graben (120 °C), corresponding to negative relief with respect to its surroundings whilst being significantly warmer than they are (80 °C). There is also an observable temperature contrast between both the northern and southern alpine forelands with the European domain in the north around 20 °C warmer (80 °C) than the Adriatic domain of the southern foreland (60 °C).

Similar trends are also noted in the 5 km depth slice. The highest temperatures are found in the western Alps (220 °C), with the eastern Alps and Upper Rhine Graben around 20 °C cooler (200 °C). At this depth, the northern foreland begins to appear warmer in the west (170 °C) and cooler in the east (150 °C). Locally higher temperatures in the northern foreland are detected to correspond to thicker deposits of sediments in the basins. Deposits of around 4 km and 5 km thickness in the Upper Rhine Graben and Molasse Basin respectively raise temperatures by 20 °C compared to the surrounding foreland. Differentiation between tectonic blocks in the northern foreland is also visible, with the Vosges Mountains in the west of the study area displaying temperatures similar (170 °C) to those of the surrounding foreland, whilst the adjacent Black Forest appears cooler (155 °C). The Bohemian Massif in the east of the study area appears warmer (160 °C) than its surroundings. Such changeable lateral temperature variations are not widely noticed in the results from the southern foreland. Temperatures instead increase gradually moving westwards, from the coolest modelled values below the Adriatic Sea (130 °C), towards the thicker sedimentary deposits of the Po Basin (140 °C).

At a depth of 10 km, the warmest domain in the model (350 °C) corresponds to the location of the Brianconnais terrane, represented by a significantly thickened upper crust (30 km) in the structural model. Thinner upper crust immediately northwards (15 km thick) can be seen in the results as an area of lower temperatures (280 °C). Whilst not representing a zone of significant crustal thinning, the Giudicarie Line marks a thermal boundary within the Alps with crust 30 °C warmer (320 °C) in the West than in the East (290 °C). However, the Tauern Window represents an exception, lying east of the Guidicarie line it is indicated by a region of elevated temperatures (330 °C) that also corresponds to a thickened upper crust. The Bohemian Massif represents a thicker upper crust (28 km) than its surroundings and also possesses warmer temperatures (310 °C), whilst contrastingly the Black Forest also shows thickened upper crust but represents colder temperatures (260 °C). The coolest temperatures in the model still occur below the Adriatic Sea (225 °C), warming inland towards the Po Basin (250 °C), with both regions encompassing an area of significantly thinned upper crust (6 km). The northern foreland again displays a trend of warming westwards, with the western Molasse Basin appearing ~40 °C warmer (300 °C) than its eastern part (260 °C). The Upper Rhine Graben is no longer one of the hottest regions at this depth level (290 °C).

At 20 km below sea level, higher temperatures correlate less to high topographies with the majority of the Alpine orogen of a similar temperature to its northern foreland, and no observable links exist between thicknesses of sediment and temperature. However, the correlation between temperature and thickness of the upper crust is noticeable, with the Brianconnais terrane the hottest region of the model (560 °C). Besides the Brianconnais terrane, the next warmest region lies in the western Molasse Basin, south of the Vosges Mountains. Temperatures there reach 540 °C and correspond to the shallowest region of the LAB (70 km), whereas below the coldest point of the model, in the Adriatic Sea (390 °C), the LAB is deepest (140 km). At this depth level the European crust still appears warmer than the Adriatic crust, with the LAB also shallower in general below Europe than Adria.

3.2. Model parameterisation and validation

The thermal properties used to achieve the best fit thermal field can be seen in Table. 1. Unconsolidated sediment thermal conductivities vary significantly throughout the region. In the Upper Rhine Graben values at the lower limit of the tested range (1.1 and 1.4 W/mK) were found necessary to replicate the fit of the measured temperatures as close as possible. However in other basin settings more standard values ranging from 1.8 W/mK in the Molasse Basin to 2.3 W/mK in the Po Basin were used. Standard values for consolidated sediments were found to be sufficient throughout the region (2.3 W/mK and 1E-06 W/m3). Within the upper crust, large variations of thermal properties were found between different crustal blocks. The Saxothuringian block was found to require the highest thermal conductivity (3 W/mK) and radiogenic heat production (2.6E-06 W/m3), whilst much lower values (2.4 W/mK and 1.3E-06 W/m3) were found necessary for the upper crust beneath the Po Basin. The lower crust shows almost homogeneous thermal properties (2 W/mK and 3.0E-07 W/m3) with the exception of the Saxothuringian block that again was found to require higher values (2.3 W/mK and 6.0E-07 W/m3). Different radiogenic heat productions were also found necessary for the two lithospheric mantle domains with the less dense domain in the northwest requiring higher values (3.0E-08 W/m3) than in the denser southeast domain (2.0E-08 W/m3).

The improvement of the best fit model over the initial model (using

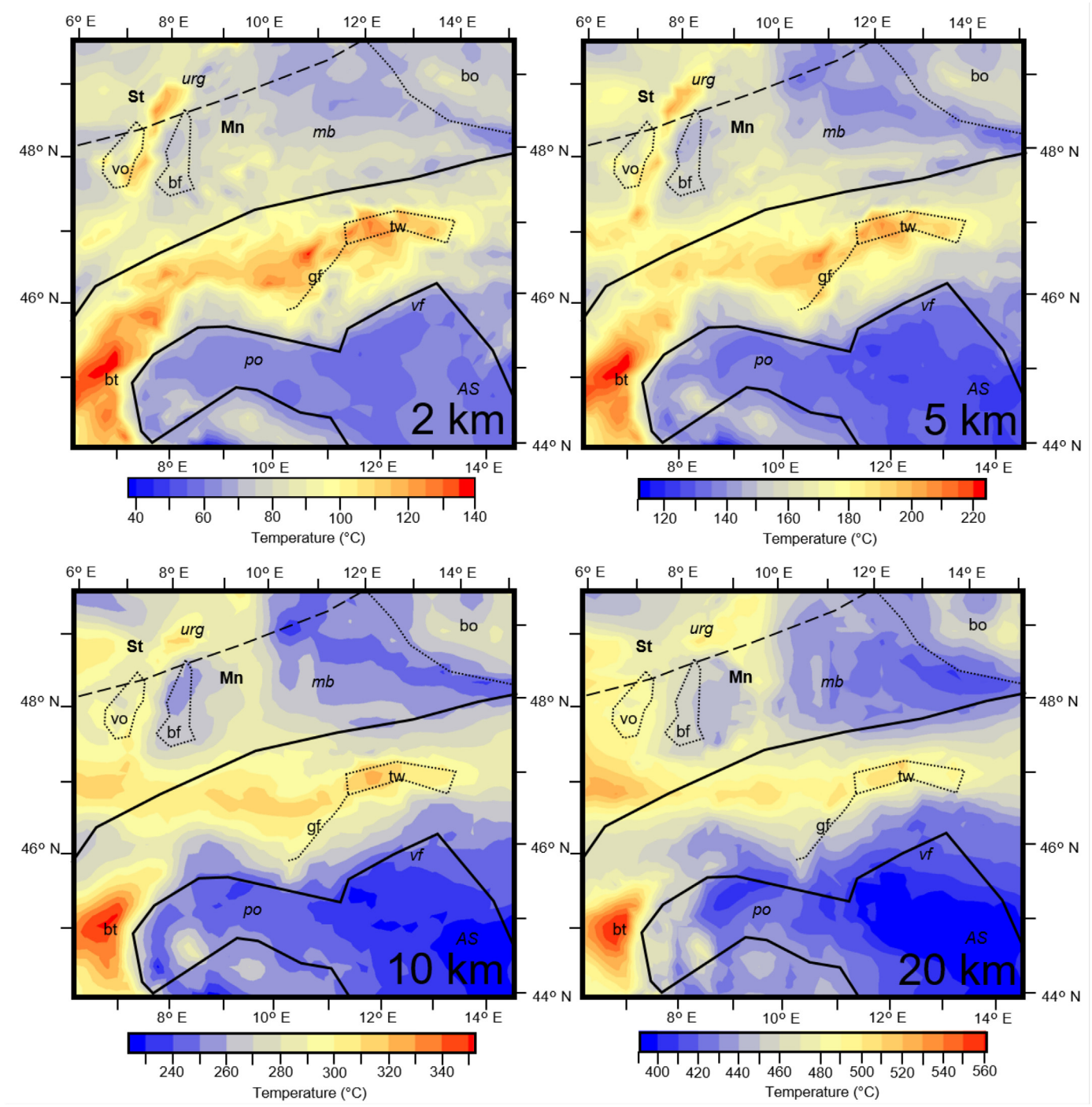

Fig. 5. Temperature maps through the final model at depths below sea level of 2 km, 5 km, 10 km and 20 km. Locations of key tectonic features are overlain (abbreviations shown in Fig. 1 caption).

the average value of the range tested in Table 1) is visualised in Fig. 6, where the difference between the modelled temperatures and measured temperatures (root mean square error) is shown at different depths. The accuracy of shallower modelled temperatures (from 2 km asl to 2 km bsl) are only slightly improved (by ~1 °C) after iterative alterations to the thermal parameters. This is because modelled temperatures at this depth were already closely representing (± 15 °C) their measurements from the initial model. However for the deepest measurements in the region (7 km), the accuracy of the best fit model (± 40 °C) is more than 20% better than the initial model (± 53 °C). Across the 8120 measurements used in the region, the root mean square error of the best fit model is 15.42 °C, significantly better than the initial model (18.55 °C).

The correlation between measured and calculated temperatures of the best fit model are plotted against depth for both the whole model and specific regions of interest (Upper Rhine Graben, Molasse Basin, Po Basin, Alps) in Figs. 7b and 8. Different regions of interest required different average geotherms to best match measured values. The highest thermal gradients are found in the sedimentary basins on the European plate with the Upper Rhine Graben requiring the highest value at 0.04 K/m, followed by the Molasse Basin with a value of 0.035 K/m. Whilst measured values are sparser in the Molasse Basin, their trend is accurately replicated by our modelling results, leaving few

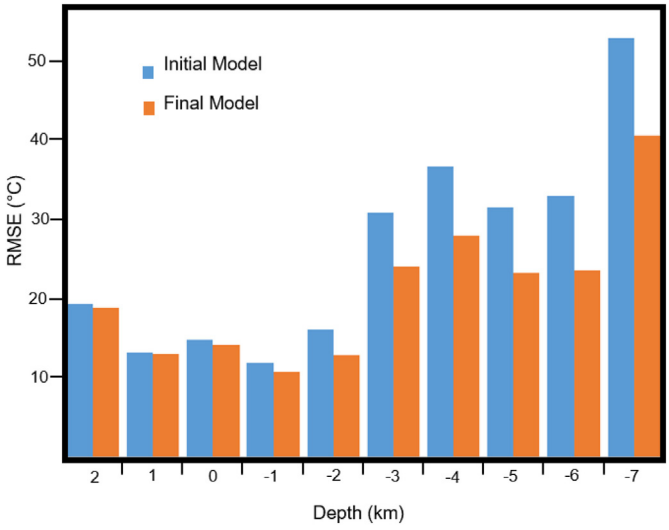

Fig. 6. Root mean square error (RMSE) of the difference between measured temperatures (°C) and the modelled temperatures (°C) from the initial and final best fit models.

outliers. Although the majority of Upper Rhine Graben measurements are well replicated, measured points in some regions deviate systematically from the regional geotherm (0.04 K/m), plotting along a localised higher geotherm (0.065 K/m). As a result, some modelled temperatures at depths of 2 km below the Upper Rhine Graben are ~60 °C cooler than their measurements suggest. Features such as local fluid movement and faults, known to affect the thermal filed in the Upper Rhine Graben (Freymark et al., 2019), are however not modelled using the present methodology.

On the Adriatic plate, geotherms are found to be significantly lower with the Po Basin showing a temperature gradient of 0.025 K/m. Covering the largest area and containing the largest amounts of measured points, the Po Basin shows a larger spread of temperatures at each depth level, however despite this, the average modelled geotherm matches the majority of measured values well, the latter not displaying any systematic deviation from the average geotherm.

The geothermal gradient found to best fit the Alpine region was equally low (0.025 K/m), like the Po Basin. The larger variation of the observed thermal gradient in the Alpine domain results from the low spatial resolution and lower accuracy of Alpine measurements. These derive from a thermal spring wellbore dataset (Luijendijk et al., 2020), which due to heat loss during transport of thermal fluids in the well represent minimum temperatures. This explains why our modelled temperatures are slightly higher than observed. Moreover, thermal springs are expressions of advective and convective heat transport - mechanisms that are not considered in our approach. Thus we aim to reproduce the overall trend of the "observed" geotherm but not its details.

3.3. Distribution of seismicity

The locations of all seismic events used are shown in Fig. 9a, with events separated into different regions (Europe, East Alps, West Alps, Adria and Apennine) to compare their relationships with modelled temperatures. Key isotherms representing temperatures in the brittle ductile transition of the dominant crustal minerals are also shown: 275 °C for wet quartz; 450 °C for feldspar; and 600 °C for wet pyroxene (Evans et al., 1990; Simpson, 1999). In the European Plate and western Alps, the majority of seismic events occur between the 275 °C and 450 °C isotherms, with most seismicity ceasing at 475 °C. However, a few isolated events occur deeper, at hotter temperatures. In the Adriatic plate and eastern Alps the correlation between seismicity and temperature is less distinct, with the majority of seismicity also occurring between the 275 °C and 450 °C isotherms, however many more events are found to temperatures of 600 °C. In the Apennine region, seismicity begins at a higher temperature (> 100 °C) and events are continuous down to the 600 °C isotherm. In both the Adriatic and Apennine regions, isolated seismicity can be seen to around 70 km depth.

Two cross sections through the structural model are shown to further illustrate the relationship between local seismicity and temperature. An East to West running section through the middle of the orogen (a-a', Fig. 10) and a North to South cross section from one foreland to the other through the orogen (b-b', Fig. 11) are marked on the map of the study area in Fig. 9a. The sediments, upper crust, lower crust and lithospheric mantle of the structural model are displayed along with all seismological epicentres that lay within a 20 km distance of the cross section. Cross section a-a' shows that in the Alps all seismicity is

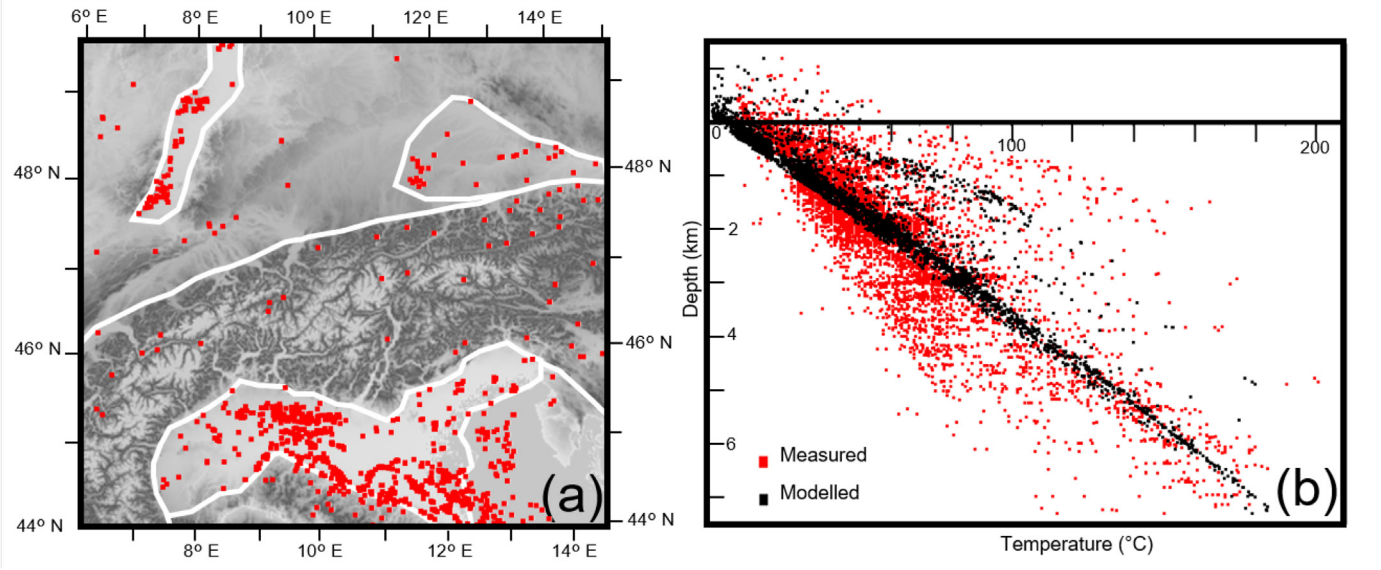

Fig. 7. a) Location of all wellbore temperatures used. Locations of regions of interest for comparing measured and modelled temperatures are bound in white. b) Comparison between measured wellbore temperatures (red) and modelled temperatures for the same points (black) plotted against depth for the whole model. (For interpretation of the references to colour in this figure legend, the reader is referred to the web version of this article.)

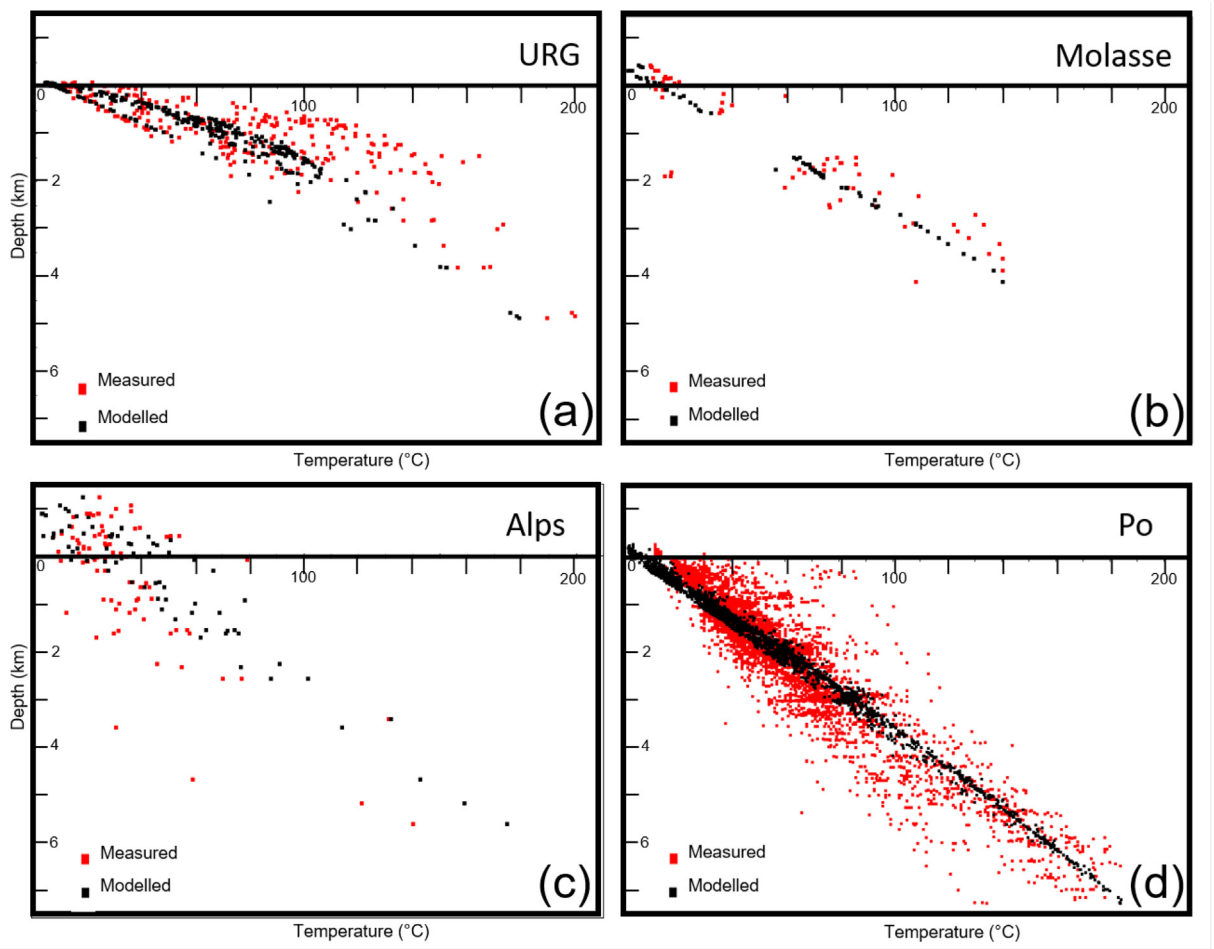

Fig. 8. a) Comparison between measured wellbore temperatures (red) and modelled temperatures at those points (black) plotted against depth for locations of interest: a) Upper Rhine Graben; b) Molasse Basin; c) the Alps; d) Po Basin. Boundaries of locations of interest are shown in Fig. 7a. (For interpretation of the references to colour in this figure legend, the reader is referred to the web version of this article.)

localised in the upper crust or Alpine nappes (shown as sediments in the cross section), with a largely aseismic lower crust also in the western Alps, where it is shallowest. Seismicity is centred around the 275 °C isotherm and does not occur at temperatures above 450 °C. Little difference can be discerned between the pattern of seismicity in the Western and Eastern Alps.

Cross section b-b' sheds light onto regional differences in the maximum depths of seismicity between different tectonic domains. As already mentioned, most seismicity within Europe and the Alps occurs at temperatures from 275 °C to 450 °C, corresponding mostly to the upper crust. With the exception of a couple of seismic events corresponding to the 600 °C isotherm at the base of the lower crust, all seismicity in Europe and the Alps terminates at the 450 °C isotherm. On the European plate, the maximum depth of seismicity is 20 km however due to raised isotherms beneath the centre of the orogen the maximum depth below the Alps is 15 km. In the Adriatic and Apennine domains, seismicity is present uniformly throughout the upper and lower crusts from 275 °C down to temperatures of 600 °C and a depth of 25 km. Additionally, the location of known subduction interfaces within the model are also overlain to show that all seismicity recorded at temperatures higher than 600 °C corresponds to known subduction interfaces (e.g. Piana Agostinetti and Faccenna, 2018; Kästle et al., 2019).

4. Discussion

4.1. Thermal field

In line with previous studies (e.g. Lucazeau and Le Douaran, 1985; Stephenson et al., 2009; Scheck-Wenderoth et al., 2014; Sippel et al., 2014), results from the sedimentary depocentres of our model show that the shallow thermal field is largely controlled by the insulating effects of sedimentary blanketing. In the 5 km below sea level depth slice (Fig. 5), temperatures are elevated by 20 °C in the Upper Rhine Graben and Molasse Basin with sedimentary thicknesses of 4 km and 5 km respectively. However, the effect of thicker sediments is less prominent in the temperature field at a crustal depth of 20 km suggesting that other factors control the temperature distribution at these crustal depths.

All main depocentres of the study area display different geothermal gradients, largely independent of their sedimentary thickness, however correlating closely with the depth of the LAB. The thermal gradient is highest in the Upper Rhine Graben (0.04 K/m) which also lies above the shallowest LAB (75 km). The higher thermal gradient in the Molasse Basin than the Po Basin, appears not solely related to the depth of the LAB as that is similar in both cases, however the upper crust below the Molasse Basin is significantly thicker than in the Po Basin, indicating radiogenic heating from the upper crust also plays a significant role. Our results demonstrate that the shallow thermal field in basins is primarily controlled by sedimentary blanketing, whilst the crustal thermal field is mostly influenced by the depth of the LAB and thickness

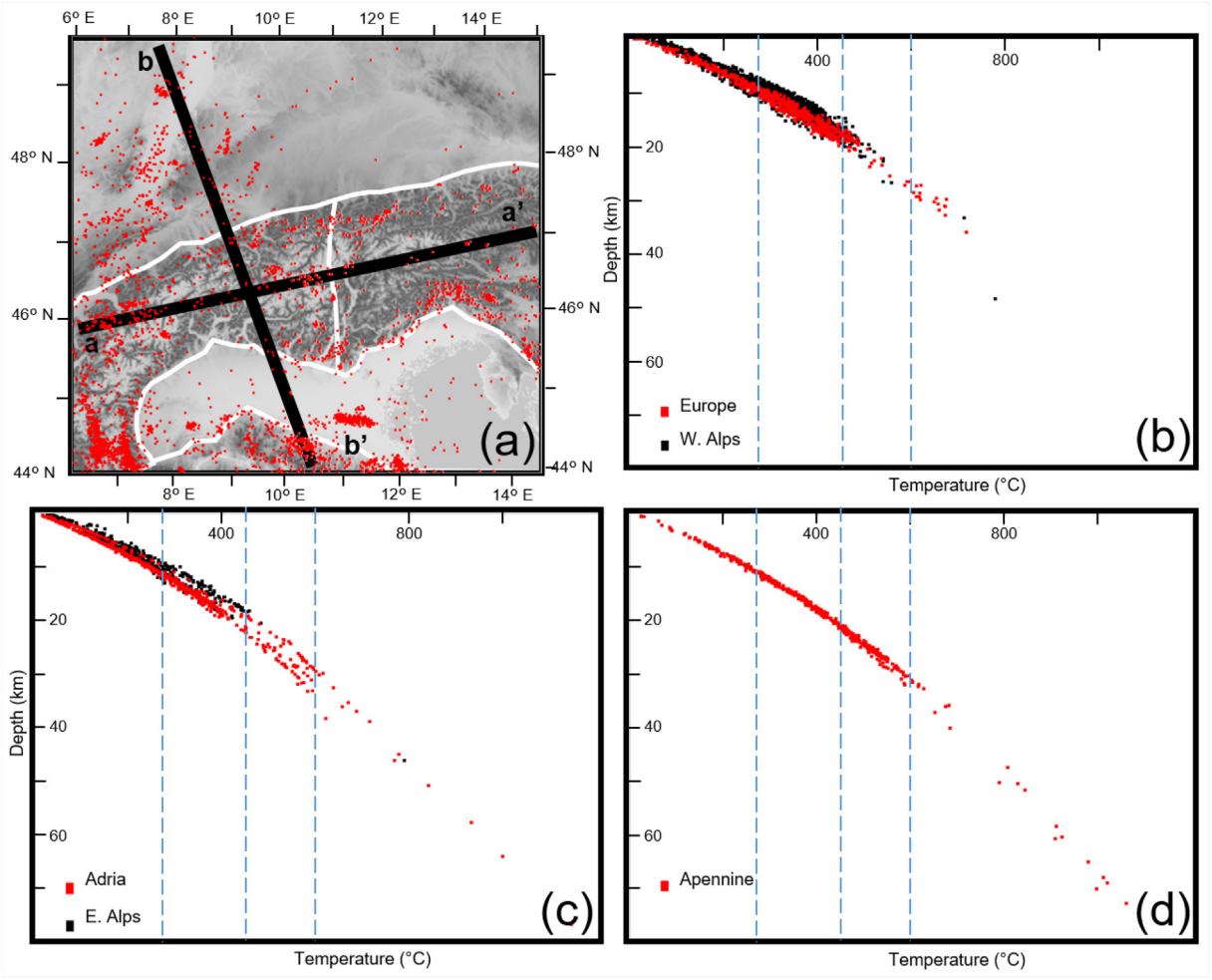

Fig. 9. Overview of seismicity data. a) Location of all seismic events used from the International Seismological Centre (International Seismological centre, 2020) between Jan 2000 and Jan 2018 with a magnitude larger than 2 shown in red dots. a-a' represents the cross section in Fig. 10, b-b' represents the cross section in Fig. 11. The white polygons delimit regions of interest, where the depth and modelled temperature of each seismic event have been shown in following panels: b) the European plate and West Alps, c) The Adriatic plate and East Alps, d) the Apennine plate. Isotherms for 275 °C, 450 °C and 600 °C are overlain as dashed blue lines. (For interpretation of the references to colour in this figure legend, the reader is referred to the web version of this article.)

of the radiogenic upper crust.

Outside of the basins, in regions of higher relief, the topographic effect is found to play a significantly larger role than sedimentary blanketing. In the 2 km below sea level depth slice (Fig. 5), the Alps appear ~80 °C warmer than their forelands, with locally up to 140 °C predicted. This results from the higher relief since 2 km below sea level translates to 5–6 km below surface in the Alps. Accordingly, even for an average thermal gradient of 0.03 K/m, temperatures in the predicted range are to be expected. In contrast, below the forelands, that are elevated less than 600 m above sea level, relatively lower temperatures are reached. To further interrogate the effect of relief on the thermal field, temperatures from 2 and 20 km below sea level and below surface

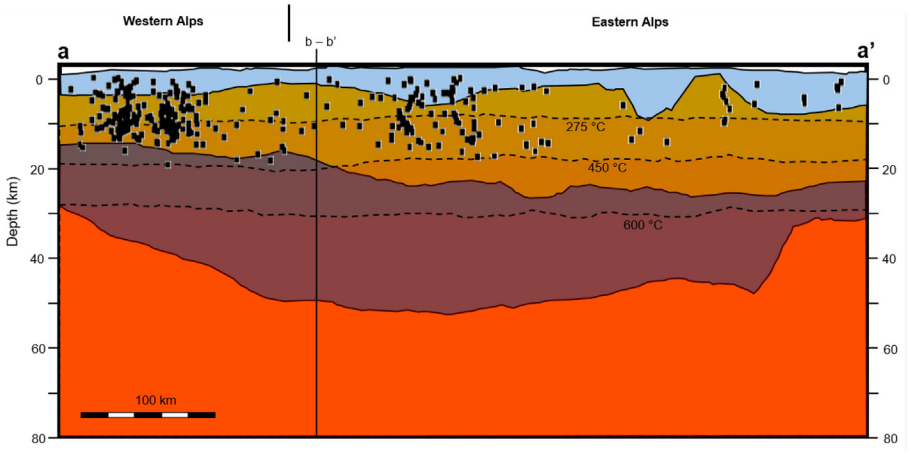

Fig. 10. A West to East cross section (a-a' in Fig. 9) through the structural model. Thickness of model layers is shown: lithospheric mantle (red), lower crust (grey), upper crust (brown) and consolidated and unconsolidated sediments (blue). Isotherms for 275 °C, 450 °C and 600 °C are overlain as dashed black lines and seismicity from the International Seismological Centre (International Seismological centre, 2020) that lay within 20 km distance of the section has been marked as black dots. (For interpretation of the references to colour in this figure legend, the reader is referred to the web version of this article.)

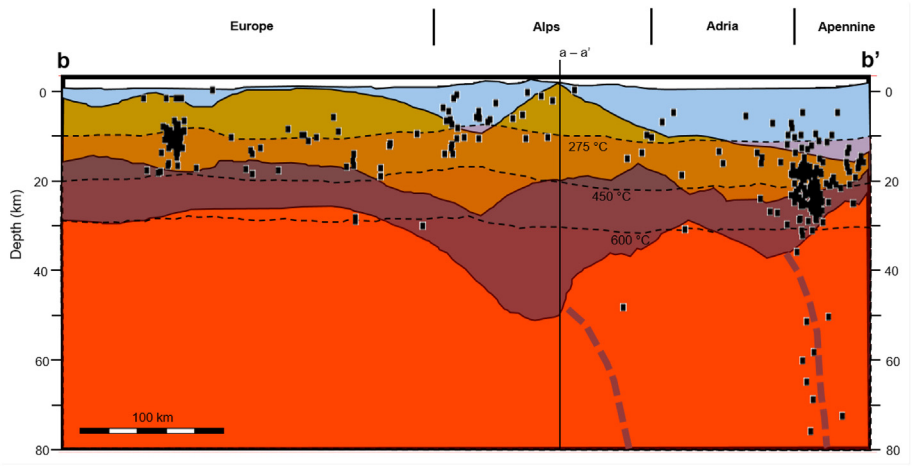

Fig. 11. A North to South cross section (b-b′ in Fig. 9) through the structural model. Thickness of model layers is shown: lithospheric mantle (red), lower crust (grey), upper crust (brown) and consolidated and unconsolidated sediments (blue). The location of unmodelled subduction interfaces have been marked as thick grey dashed lines. Isotherms for 275 °C, 450 °C and 600 °C are overlain as dashed black lines and seismicity from the International Seismological Centre (International Seismological centre, 2020) that lay within 20 km distance of the section has been marked as black dots. (For interpretation of the references to colour in this figure legend, the reader is referred to the web version of this article.)

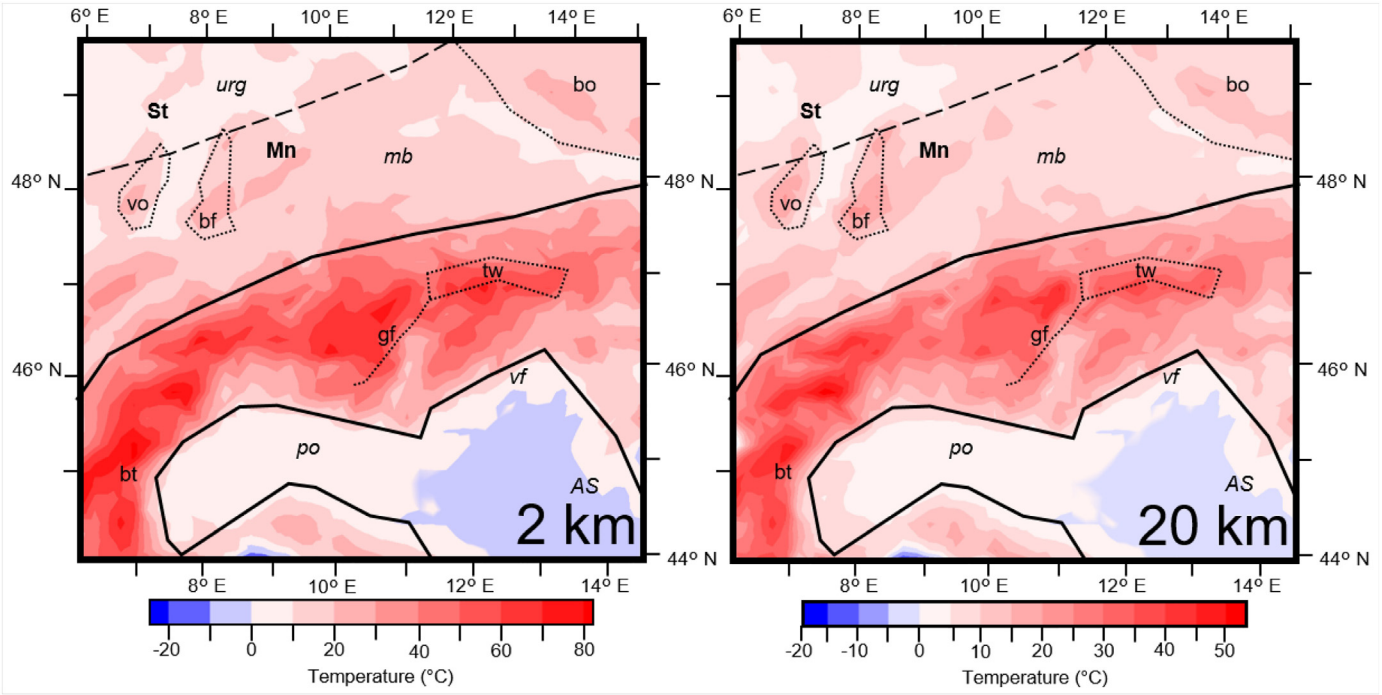

Fig. 12. Difference maps between temperature slices below sea and below surface at depths of 2 km and 20 km, showing the effect of topographic relief at either depth. Locations of key tectonic features are overlain (abbreviations shown in Fig. 1 caption).

were extracted from the model and the resulting temperature difference visualised in Fig. 12. The difference maps demonstrate that the topographic effect is indeed responsible for the largest part of the temperature difference between the orogen and forelands at shallow depths (around 80 °C at 2 km below sea level). The effect decreases with increasing depth, but is still evident at a depth of 20 km below sea level with a difference of around 55 °C.

The lessening impact of the topographic effect with depth is also mirrored by the increasing impact of upper crustal thickness on temperatures as depth increases. Areas of thicker Alpine upper crust that appear warmer than their surroundings include the Brianconnais terrane and the Tauern Window, with it also being the primary cause of the Alpine West to East cooling transition noted to correspond with the Guidicarie fault line seen in Fig. 5. In the northern Alpine foreland, the Bohemian Massif is characterised by both thick upper crust and elevated relief. However, in accordance with the results by Przybycin et al. (2015), temperatures are not particularly elevated there since the exhumed Variscan basement acts as a heat chimney in the absence of insulating sediments.

The presence of European crust thicker (27.5 km) than Adriatic crust (22.5 km) explains why the northern foreland is warmer than the southern at all depth levels. However, these temperatures also correlate with the LAB depth. The LAB deepens southwestwards, shallowest below the Upper Rhine Graben in the European domain (70 km) and deepest below the Adriatic Sea (140 km). LAB depth is also a primary driver of the observed West to East cooling of both the northern and southern forelands visible at all depth levels, and this effect also manifests in the nearby crustal blocks, with higher temperatures below the Vosges Massif compared to the adjacent Black Forest, both of which are represented by the same thermal parameters, relief and upper crustal thickness.

4.2. Lithological inferences from seismicity

Different minerals undergo brittle to ductile transition at different temperatures, (see Distribution of Seismicity section) which also act as

the lower bound to the seismogenic zone. In polymineralic rocks, i.e. almost all crustal rocks, the brittle ductile transition for different minerals in the rock is reached at different temperatures (Evans et al., 1990) allowing approximate bulk lithological assumptions to be made based on the depths seismicity is present to in the different regions of the model. Across the European and Alpine domains, the upper crust shows a cut off in seismicity across the 450 °C isotherm, with seismicity centered around the 275 °C isotherm suggesting a bulk quartz-feldspathic lithology whilst the lower crust remains largely aseismic. Such lithology would also be consistent with observed seismic velocities and modelled densities in these domains (Spooner et al., 2019 and references therein). Seismicity is only present in the European foreland lower crust under 2 conditions: either (1) at temperatures cooler than 450 °C, suggesting a less mafic lithology than would be expected, which is supported with the results of previous work (Spooner et al., 2019), where the European lower crust is shown to have lower density (2800 kg/m3) than typical lower crust; or (2) related to European slab rollback under the Central Alps (Singer et al., 2014)

Expected limitations of the steady state methodology are observed through overestimated temperatures at subduction interfaces in the region. Although seismicity is known to terminate around 600 °C in these settings (Emmerson and McKenzie, 2007), we observe events occurring at modelled temperatures in excess of 1000 °C, where the Adriatic crust subducts below the northern Apennines. This is due to the crust being subducted faster than it can reach thermal equilibrium with the surrounding warmer mantle, requiring in the region of 1.6 ma after subduction has ended to achieve equilibrium (Fairley, 2016). However, as this effect is not accounted for in the steady state model, seismicity appears to occur at higher temperatures than would be expected.

Outside of subduction interfaces, seismicity occurs to the 600 °C isotherm in the Adriatic and Apennine upper and lower crusts, indicating a bulk lithology with higher pyroxene content for both than the European crusts. This is also consistent with the results of density modelling, where the southern foreland Adriatic crust is shown to be in general denser (2800 kg/m3) than the European crust (2750 kg/m3). Due to the topographic effect and the radiogenic heating of the thickened upper crust below the orogen, much of the alpine lower crust is hotter than 600 °C and seismicity is predominantly absent.

We find that in general the Adriatic upper crustal domain requires lower radiogenic heat production (1.30E-06 W/m3) and thermal conductivity (2.4 W/mK) than the European upper crustal domains (1.3–2.6E-06 W/m3 and 2.4–3 W/mK), a trend visible even though each region is parameterised by multiple domains. The radiogenic heat values required to fit observations also indicate a more mafic (e.g. Hasterok and Webb, 2017) composition for the Adriatic crust than the European, which is consistent with the bulk lithology derived from density modelling or seismic velocities.

Indications that the Adriatic crust is more mafic in composition than the European crust are therefore supported by: 1) seismicity distribution relative to the thermal field and the brittle ductile transition of crustal minerals; 2) thermal properties necessary to fit measured wellbore temperatures; and 3) densities necessary to fit the measured gravity field. These bulk lithological observations in conjunction with the calculated temperatures and the previous 3D density-structural model of the region, can be used to shed light on the lateral changes in crustal strength within the Alps and their forelands, helping to explain the observed patterns of deformation and to create more accurate strength profiles throughout the region.

4.3. Importance of limitations

The local mismatch of observed shallow temperatures with those predicted by a conductive heat transport simulation suggests that hydrothermal convection in the Upper Rhine Graben significantly effects the shallow thermal field of the region. This is in line with other works (e.g. Bächler et al., 2003; Freymark et al., 2017; Koltzer et al., 2019) that also suggested these effects are negligible below 10 km depth. Thus our findings for the relationships between observed crustal seismicity and the deep thermal field are robust. However, none of the other thermal effects unaccounted for in a steady state thermal model (examples listed in the Methodological Limitations section) are noticed during an interrogation of our results. Whilst their impact is likely present, they are not of a magnitude that could result in visible systematic offset between measured and modelled temperatures.

Whilst an increase in resolution of 3D structural model, is nevertheless desirable, the largest limiting factor to the thermal field generated is the availability of measured temperature data. Even with a course 20 km × 20 km structural model resolution, as can be seen in Fig. 7a, large portions of the orogen and either foreland lack any measured temperatures. Therefore, without an increase in coverage of measured temperatures an increase of model resolution would not result in a more accurate thermal field. To interrogate this, work is underway to quantify the sensitivity of thermal parameters used in this model in relation to the spacing of measured temperatures available.

4.4. Global applicability

Observations made during this study of physical controls on the modelled thermal field remain applicable to a wide array of tectonic settings worldwide. We find that in central mountain belt settings, the thickness of the radiogenic upper crust, depth to the LAB and topographic effect have the largest impact on the thermal field, with a relief of 4 km raising temperatures by 50 °C at 20 km depth. In conjunction with associated upper crustal thickening resulting from orogenesis these raised temperatures result in maximum depths of seismicity more than 5 km shallower than in the forelands.

In basin settings, we find that in the absence of relief, the thickness of sedimentary deposits, the depth to the LAB and the magnitude of crustal thinning have the largest impact on the thermal field. The results also suggest that the advection of hot fluids and associated influence of localised faults in these regions are an important factor unaccounted for in this study. Similarly, in subduction zones we see that it is crucial to consider the transient thermal effects, such as the time taken for the downgoing crust to thermally equilibrate.

Inferences on lithology from the maximum observed depths of seismicity, align well with previous observations on bulk densities from gravity modelling, an indication that seismicity distribution in conjunction with a 3D thermal field can be used to gain a rough first order estimate of the bulk lithology of a region. These findings are not region specific and as seismicity represents a global issue, the techniques this study utilises can be applied worldwide in order to interrogate the relationship between seismicity and the lithospheric thermal field as a first step to quantifying seismic hazard.

5. Summary

By creating the first 3D steady state thermal field of the Alps and their forelands, validated with wellbore temperature measurements, that uses different thermal parameters for different tectonic domains, insights were gained into the controlling factors on the thermal field and lithological indications of each crustal block. The findings suggest that the shallow thermal field (0–10 km) is largely controlled by sedimentary blanketing or topographic effects, with the central orogen appearing 80 °C warmer than its forelands at a depth of 2 km below sea level and temperatures in the centre of the Molasse Basin 20 °C warmer than at the edges. We also show how the deeper thermal field (10–20 km) appears controlled by the LAB depth and the radiogenic contribution of the upper crust, with thickness and lithology (magnitude of radiogenic heat production) important influencing factors at crustal depths.

The European upper crustal domains require higher radiogenic heat productions and thermal conductivities (1.3–2.6E-06 W/m3 and

2.4–3 W/mK) than the Adriatic upper crust (1.30E-06 W/m3 and 2.4 W/mK). In conjunction with density observations, we use these thermal parameters to suggest the Adriatic crust is more mafic than the European. This is strengthened by observed differences in the clustering of seismicity at suspected brittle ductile transitions, with the Adriatic and Apennine plates demonstrating seismicity to higher temperatures, indicating a larger percentage of pyroxene than in the European crust.

Declaration of Competing Interest

None.

Acknowledgements

The authors would like to thank the Deutsche Forschungsgemeinschaft (DFG) for funding the Mountain Building Processes in Four Dimensions (4-D-MB) SPP that this work was produced as part of. We would also like to thank Stanislaw Mazur and 2 other anonymous reviewers for their suggested improvements to the manuscript.

Declaration of Competing Interest

The authors declare that they have no known competing financial interests or personal relationships that could have appeared to influence the work reported in this paper.

References

Allen, P., Allen, J., 2013. Basin Analysis, 3rd ed. Wiley, Somerset.
Amante, C. and Eakins, B. W. 2020 ETOPO1 1 Arc-Minute Global Relief Model: Procedures, Data Sources and Analysis. NOAA Technical Memorandum NESDIS NGDC-24, National Geophysical Data Center, NOAA, doi:https://doi.org/10.1594/PANGAEA.769615, 2009.
Babuška, V., Plomerová, J., 1992. The lithosphere in Central Europe – seismological and petrological aspects. Tectonophysics 207, 141–163. https://doi.org/10.1016/0040-1951(92)90475-l.
Bächler, D., Kohl, T., Rybach, L., 2003. Impact of graben-parallel faults on hydrothermal convection—Rhine Graben case study. Phys. Chem.Earth, Parts A/B/C 28 (9–11), 431–441. https://doi.org/10.1016/s1474-7065(03)00063-9.
Bleibinhaus, F., Gebrande, H., 2006. Crustal structure of the Eastern Alps along the TRANSALP profile from wide-angle seismic tomography. Tectonophysics 414 (1–4), 51–69. https://doi.org/10.1016/j.tecto.2005.10.028.
Böhm, R., Auer, I., Schöner, W., Ganekind, M., Gruber, C., Jurkovic, A., Orlik, A., Ungersböck, M., 2009. Eine neue Webseite mit instrumentellen Qualitäts-Klimadaten für den Grossraum Alpen zurück bis 1760. Wiener Mitteilungen Band 216: Hochwässer: Bemessung, Risikoanalyse und Vorhersage.
Cacace, M., Jacquey, A., 2017. Flexible parallel implicit modelling of coupled thermal–hydraulic–mechanical processes in fractured rocks. Solid Earth 8 (5), 921–941. https://doi.org/10.5194/se-8-921-2017.
Dèzes, P., Schmid, S., Ziegler, P., 2004. Evolution of the European Cenozoic Rift System: interaction of the Alpine and Pyrenean orogens with their foreland lithosphere. Tectonophysics 389, 1–33. https://doi.org/10.1016/j.tecto.2004.06.011.
Ehlers, T., 2005. Crustal thermal processes and the interpretation of thermochronometer data. Rev. Mineral. Geochem. 58 (1), 315–350. https://doi.org/10.2138/rmg.2005.58.12.
Ehlers, T., Chapman, D., 1999. Normal fault thermal regimes: conductive and hydrothermal heat transfer surrounding the Wasatch fault, Utah. Tectonophysics 312 (2–4), 217–234. https://doi.org/10.1016/s0040-1951(99)00203-6.
Emmerson, B., McKenzie, D., 2007. Thermal structure and seismicity of subducting lithosphere. Phys. Earth Planet. Inter. 163 (1–4), 191–208. https://doi.org/10.1016/j.pepi.2007.05.007.
Evans, B., Fredrich, J., Wong, T., 1990. The brittle-ductile transition in rocks: recent experimental and theoretical progress. Brittle-Ductile Transit. Rocks 1–20. https://doi.org/10.1029/GM056p0001.
Fairley, J., 2016. Models and Modeling: An Introduction for Earth and Environmental Scientists. Wiley-Blackwell.
Fan, Y., van den Dool, H., 2008. A global monthly land surface air temperature analysis for 1948-present. J. Geophys. Res. 113, D01103. https://doi.org/10.1029/2007JD008470.
Fox, M., Herman, F., Willett, S., Schmid, S., 2016. The Exhumation history of the European Alps inferred from linear inversion of thermochronometric data. Am. J. Sci. 316 (6), 505–541. https://doi.org/10.2475/06.2016.01.
Franke, W., 2000. The mid-European segment of the Variscides: tectonostratigraphic units, terrane boundaries and plate tectonic evolution. Geol. Soc. Lond. Special Publications 179, 35–61. https://doi.org/10.1144/gsl.sp.2000.179.01.05.
Freymark, J., Sippel, J., Scheck-Wenderoth, M., Bär, K., Stiller, M., Fritsche, J., Kracht, M., 2017. The deep thermal field of the Upper Rhine Graben. Tectonophysics 694, 114–129. https://doi.org/10.1016/j.tecto.2016.11.013.
Freymark, J., Bott, J., Cacace, M., Ziegler, M., Scheck-Wenderoth, M., 2019. Influence of the Main Border Faults on the 3D Hydraulic Field of the Central Upper Rhine Graben. Geofluids 2019, 1–21. https://doi.org/10.1155/2019/7520714.
Frisch, W., 1979. Tectonic progradation and plate tectonic evolution of the Alps. Tectonophysics 60 (3–4), 121–139. https://doi.org/10.1016/0040-1951(79)90155-0.
Geissler, W., Sodoudi, F., Kind, R., 2010. Thickness of the central and eastern European lithosphere as seen by S receiver functions. Geophys. J. Int. https://doi.org/10.1111/j.1365-246x.2010.04548.x.
Handy, M., Schmid, M., Bousquet, R., Kissling, E., Bernoulli, D., 2010. Reconciling plate-tectonic reconstructions of Alpine Tethys with the geological–geophysical record of spreading and subduction in the Alps. Earth-Sci. Rev. 102, 121–158. https://doi.org/10.1016/j.earscirev.2010.06.002.
Hasterok, D., Webb, J., 2017. On the radiogenic heat production of igneous rocks. Geosci. Front. 8 (5), 919–940. https://doi.org/10.1016/j.gsf.2017.03.006.
Hyndman, R., Wang, K., Yamano, M., 1995. Thermal constraints on the seismogenic portion of the southwestern Japan subduction thrust. J. GeophyS. Res. Solid Earth 100 (B8), 15373–15392. https://doi.org/10.1029/95jb00153.
International Seismological Centre, 2020. On-line Bulletin. https://doi.org/10.31905/D808B830.
Kästle, E., Rosenberg, C., Boschi, L., Bellahsen, N., Meier, T., El-Sharkawy, A., 2019. Slab Break-offs in the Alpine Subduction Zone. Solid Earth Discuss. 1–16. https://doi.org/10.5194/se-2019-17.
Koltzer, N., Scheck-Wenderoth, M., Bott, J., Cacace, M., Frick, M., Sass, I., Fritsche, J., Bär, K., 2019. The effects of regional fluid flow on deep temperatures (Hesse, Germany). Energies 12 (11), 2081. https://doi.org/10.3390/en12112081.
Limberger, J., van Wees, J., Tesauro, M., Smit, J., Bonté, D., Békési, E., Pluymaekers, M., Struijk, M., Vrijlandt, M., Beekman, F., Cloetingh, S., 2018. Refining the thermal structure of the European lithosphere by inversion of subsurface temperature data. Glob. Planet. Chang. 171, 18–47. https://doi.org/10.1016/j.gloplacha.2018.07.009.
Locarnini, R.A., Mishonov, A.V., Antonov, J.I., Boyer, T.P., Garcia, H.E., Baranova, O.K., Zweng, M.M., Paver, C.R., Reagan, J.R., Johnson, D.R., Hamilton, M., Seidov, D., 2013. World Ocean Atlas 2013, Volume 1: Temperature. S. Levitus, Ed., A. Mishonov Technical Ed.; NOAA Atlas NESDIS 73, 40 pp. .
Lucazeau, F., Le Douaran, S., 1985. The blanketing effect of sediments in basins formed by extension: a numerical model. Application to the Gulf of Lion and Viking graben. Earth Planet. Sci. Lett. 74 (1), 92–102. https://doi.org/10.1016/0012-821x(85)90169-4.
Luijendijk, E., Winter, T., Köhler, S., Ferguson, G., von Hagke, C., Scibek, J., 2020. Using Thermal Springs to Quantify Groundwater flow and its Thermal Footprint in the Alps and North American Orogens. (Manuscript in preparation, 2020).
Meeßen, C., 2018. VeloDT. https://doi.org/10.5281/zenodo.1172628.
Mey, J., Scherler, D., Wickert, A., Egholm, D., Tesauro, M., Schildgen, T., Strecker, M., 2017. Erratum: corrigendum: glacial isostatic uplift of the European Alps. Nat. Commun. 8 (1). https://doi.org/10.1038/ncomms16138.
Nocquet, J., Calais, E., 2004. Geodetic measurements of crustal deformation in the Western Mediterranean and Europe. Pure Appl. Geophys. 161, 661–681. https://doi.org/10.1007/s00024-003-2468-z.
Pesaresi, M., Ehrlich, D., Kemper, T., Siragusa, A., Florczyk, A.J., Freire, S., Corbane, C., 2017. Atlas of the Human Planet 2017: Global Exposure to Natural Hazards, EUR 28556 EN. https://doi.org/10.2760/19837.
Piana Agostinetti, N., Faccenna, C., 2018. Deep structure of Northern Apennines subduction Orogen (Italy) as revealed by a joint interpretation of passive and active seismic data. Geophys. Res. Lett. 45 (9), 4017–4024. https://doi.org/10.1029/2018gl077640.
Priestly, K., McKenzie, D., 2006. The thermal structure of the lithosphere from shear wave velocities. Earth Planet. Sci. Lett. 244 (1–2), 285–301. https://doi.org/10.1016/j.epsl.2006.01.008.
Przybycin, A., Scheck-Wenderoth, M., Schneider, M., 2014. Assessment of the isostatic state and the load distribution of the European Molasse basin by means of lithospheric-scale 3D structural and 3D gravity modelling. Int. J. Earth Sci. 104 (5), 1405–1424. https://doi.org/10.1007/s00531-014-1132-4.
Przybycin, A., Scheck-Wenderoth, M., Schneider, M., 2015. The 3D conductive thermal field of the North Alpine Foreland Basin: influence of the deep structure and the adjacent European Alps. Geotherm. Energy 3 (1). https://doi.org/10.1186/s40517-015-0038-0.
Restivo, A., Bressan, G., Sugan, M., 2016. Stress and strain patterns in the venetian Prealps (North-Eastern Italy) based on focal-mechanism solutions. B. Geofis. Teor. Appl. 57, 13–30.
Schaeffer, A., Lebedev, S., 2013. Global shear speed structure of the upper mantle and transition zone. Geophys. J. Int. 194 (1), 417–449. https://doi.org/10.1093/gji/ggt095.
Scheck-Wenderoth, M., Cacace, M., Maystrenko, Y., Cherubini, Y., Noack, V., Kaiser, B., Sippel, J., Björn, L., 2014. Models of heat transport in the central European Basin System: Effective mechanisms at different scales. Mar. Pet. Geol. 55, 315–331. https://doi.org/10.1016/j.marpetgeo.2014.03.009.
Schmid, S., Fügenschuh, B., Kissling, E., Schuster, R., 2004. Tectonic map and overall architecture of the Alpine orogen. Eclogae Geol. Helv. 97 (1), 93–117. https://doi.org/10.1007/s00015-004-1113-x.
Serpelloni, E., Vannucci, G., Anderlini, L., Bennett, R., 2016. Kinematics, seismotectonics and seismic potential of the eastern sector of the European Alps from GPS and seismic deformation data. Tectonophysics 688, 157–181. https://doi.org/10.1016/j.tecto.2016.09.026.

Simpson, F., 1999. Surv. Geophys. 20 (3/4), 201–227. https://doi.org/10.1023/A:1006641922180.

Singer, J., Diehl, T., Husen, S., Kissling, E., Duretz, T., 2014. Alpine lithosphere slab rollback causing lower crustal seismicity in northern foreland. Earth Planet. Sci. Lett. 397, 42–56. https://doi.org/10.1016/j.epsl.2014.04.002.

Sippel, J., Scheck-Wenderoth, M., Lewerenz, B., Klitzke, P., 2014. Deep vs. shallow controlling factors of the crustal thermal field insights from 3D modelling of the Beaufort-Mackenzie Basin (Arctic Canada). Basin Res. 27 (1), 102–123. https://doi.org/10.1111/bre.12075.

Smith, L., Chapman, D., 1983. On the thermal effects of groundwater flow: 1. Regional scale systems. J. Geophys. Res. 88 (B1), 593. https://doi.org/10.1029/jb088ib01p00593.

Spooner, C., Scheck-Wenderoth, M., Götze, H., Ebbing, J., Hetényi, G., 2019. Density distribution across the Alpine lithosphere constrained by 3-D gravity modelling and relation to seismicity and deformation. Solid Earth 10 (6), 2073–2088. https://doi.org/10.5194/se-10-2073-2019.

Stephenson, R., Egholm, D., Nielsen, S., Stovba, S., 2009. Role of thermal refraction in localizing intraplate deformation in southeastern Ukraine. Nat. Geosci. 2 (4), 290–293. https://doi.org/10.1038/ngeo479.

Sternai, P., Sue, C., Husson, L., Serpelloni, E., Becker, T., Willett, S., Faccenna, C., Di Giulio, A., Spada, G., Jolivet, L., Valla, P., Petit, C., Nocquet, J., Walpersdorf, A., Castelltort, S., 2019. Present-day uplift of the European Alps: evaluating mechanisms and models of their relative contributions. Earth Sci. Rev. 190, 589–604. https://doi.org/10.1016/j.earscirev.2019.01.005.

Tesauro, M., Kaban, M., Cloetingh, S., 2009. A new thermal and rheological model of the European lithosphere. Tectonophysics 476 (3–4), 478–495. https://doi.org/10.1016/j.tecto.2009.07.022.

Trumpy, E., Manzella, A., 2017. Geothopica and the interactive analysis and visualization of the updated Italian National Geothermal Database. Int. J. Appl. Earth Obs. Geoinf. 54, 28–37. https://doi.org/10.1016/j.jag.2016.09.004.

Vrabec, M., Fodor, L., 2006. Late Cenozoic tectonics of Slovenia: structural styles at the northeastern corner of the Adriatic microplate, the adria microplate: gps geodesy, tectonics and hazards. In: Pinter, N., Grenerczy, G., Weber, J., Stein, S., Medak, D. (Eds.), Nato Scie Series, IV, Earth and Environmental Science. Vol. 61. Springer, Dordrecht, pp. 151–158.